Supplemental Figure Legends

Figure S1. The PatA analogue, DMPatA, is a potent inducer of eIF4A1:poly $(AG)_8$ RNA clamping, *Related to Figure 1*. **a.** Left panel: Polarization values obtained with wt eIF4A1 (10 μM) in the presence of DMPatA (2.5 μM) or CR-1-31-B (10 μM) and FAM-labeled RNA (10 nM). Reactions were assembled in binding buffer (14.4 mM HEPES-NaOH [pH 8], 108 mM NaCl, 14.4% glycerol, 0.1% DMSO, 2 mM DTT) in the presence or absence of 1 mM $MgCl_2$/1mM ATP. n=4 ± SEM. P values were calculated using one-way ANOVA. Right panel: Results of filter binding assay obtained with wt eIF4A1 (2.5 μM) in the absence or presence of 1 mM $MgCl_2$/1mM ATP and DMPatA (2.5 μM) or CR-1-31-B (10 μM). Radioactive [^{32}P]-poly$(AG)_8$ RNA (100,000 cpm) was used as input. n=3 ± SEM. P values were calculated using one-way ANOVA. **b.** ATPase activity of pre-clamped eIF4A1:RNA:DMPatA complexes. eIF4A1, poly $(AG)_8$ RNA, 0.5 mM cold ATP with or without DMPatA (2.5 uM) were pre-incubated at RT for 30 min, after which 1 μCi γ-^{32}P-ATP (3000 Ci/mmol) was added and ATP hydrolysis monitored for 120 mins. n=3± SEM.

Figure S2. Superpositions of the eIF4A structure determined herein with those of eIF4A1:RocA (PDB 5ZC9) and the Drosophila DEAD box helicase, Vasa (PDB 2DB3), *Related to Figure 2*. **a.** The similarity to Vasa indicates that DMPatA and RocA are likely binding to the pre-existing closed conformation induced by binding of RNA and AMP-PNP. Root mean squared deviations (r.m.s.d) derived from the number of corresponding Cα atoms in parentheses are indicated. **b, c** Simulated annealing Fo-Fc omit maps for (**a**) RNA and (**b**) DMPatA contoured at 2.5σ. An annealing temperature of 2500K was used.

Figure S3. Comparison of interactions between eIF4A1 and DMPatA or RocA, *Related to Figure 2*. **a.** Ligplot schematic diagram showing DMPatA and RocA contacts to eIF4A1. **b.** RocA-eIF4A1 and RocA-RNA interactions as defined by Iwasaki et al. (2019) and based on PDB 5ZC9.

Figure S4. RNA binding of eIF4A1 mutants with substitutions at DMPatA interacting amino acids, *Related to Figure 4*. **a.** Coomassie-stained polyacrylamide gel of the protein preparations used in this study. **b.** Polarization values obtained with the indicated proteins when incubated with FAM-labelled $(AG)_8$ RNA and ATP. n=3 ± SEM. **c.** Polarization values obtained with wt eIF4A1 and D198K with FAM-poly $(AG)_8$ RNA in the presence of either DMPatA (2.5 μM) or CR-1-31-B (10 μM). n=5 ± SEM. P values were calculated using two-way ANOVA. **d.** Polarization values obtained with wt eIF4A1, R282K, and D305A mutants with FAM- labelled $(AG)_8$ RNA in the presence of DMPatA (2.5 μM). n=5 ± SEM.

Figure S5. Schematic diagram illustrating construction and validation of *EIF4A2*$^{-}$ and *EIF4A1*^{F163L} *EIF4A2*$^{-}$ eHAP1 cells, *Related to Figure 4*. **a.** The sequence within *EIF4A2* exon 5 targeted by the indicated sgRNA (bold) is shown. The PAM is shaded orange and the resulting nucleotide change within *EIF4A2* identified in a clonal isolate consisted of a 2 base pair insertion, resulting in early termination of translation (amino acid changes are indicated in blue and * denotes the location of the stop codon). For *EIF4A1*^{F163L} engineering, the targeted codon is highlighted by a dashed orange box and the engineered change in the donor ssODN is indicated in green. A clonal isolate was expanded and the presence of the F163L mutation confirmed by Sanger sequencing of a PCR product obtained from amplifying exon 5. Shown are Western blots of protein extracts isolated from the indicated cells assessing eIF4A1 and eIF4A2 levels. **b.** Cytotoxicity of CR-1-31-B towards wt (blue circles), *EIF4A2*$^{-}$ (orange squares), and *EIF4A1*^{F163L}*EIF4A2*$^{-}$ (green triangles) eHAP1 cells. Cell were exposed to the

indicated concentrations for 2 days and viability was measured using the SRB assay. The IC_{50}'s of CR-1-31-B towards the test cell lines were: CR-1-31-B/eHAP, 0.3 ± 0.07 nM; CR-1-31-B/*EIF4A2*$^{-}$, 0.37 ± 0.08 nM; CR-1-31-B /*EIF4A1*^{F163L}*EIF4A2*$^{-}$, >115 nM; n = 3 ± SEM.

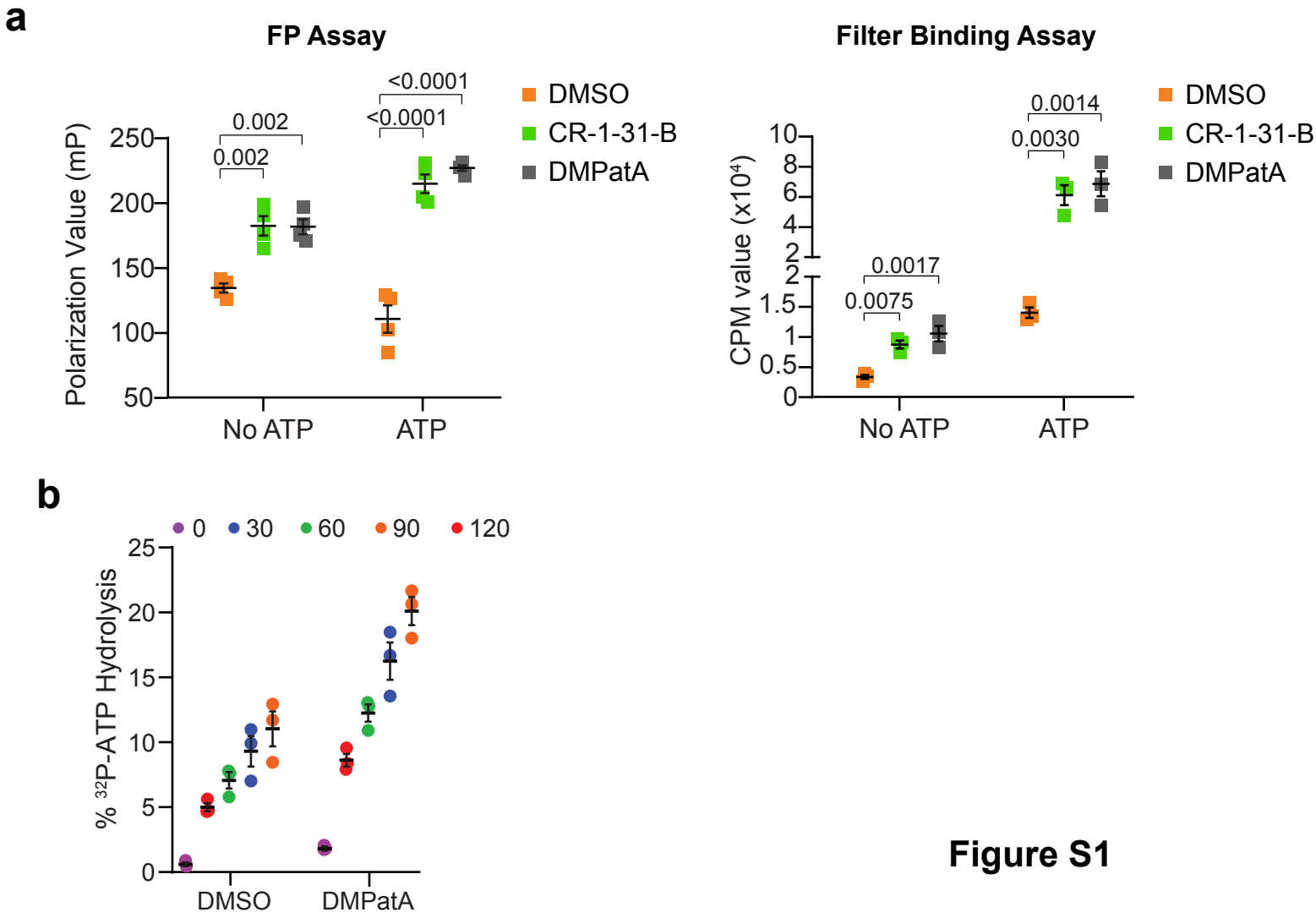
a
FP Assay
Polarization Value (mP)
250
200
150
100
50
0.002
0.002
<0.0001
<0.0001
No ATP
ATP
DMSO
CR-1-31-B
DMPatA
Filter Binding Assay
CPM value (x10⁴)
10
8
6
4
2
2
1.5
1
0.5
0
0.0017
0.0075
0.0014
0.0030
No ATP
ATP
DMSO
CR-1-31-B
DMPatA
b
0
30
60
90
120
% ³²P-ATP Hydrolysis
25
20
15
10
5
0
DMSO
DMPatA

Figure S1

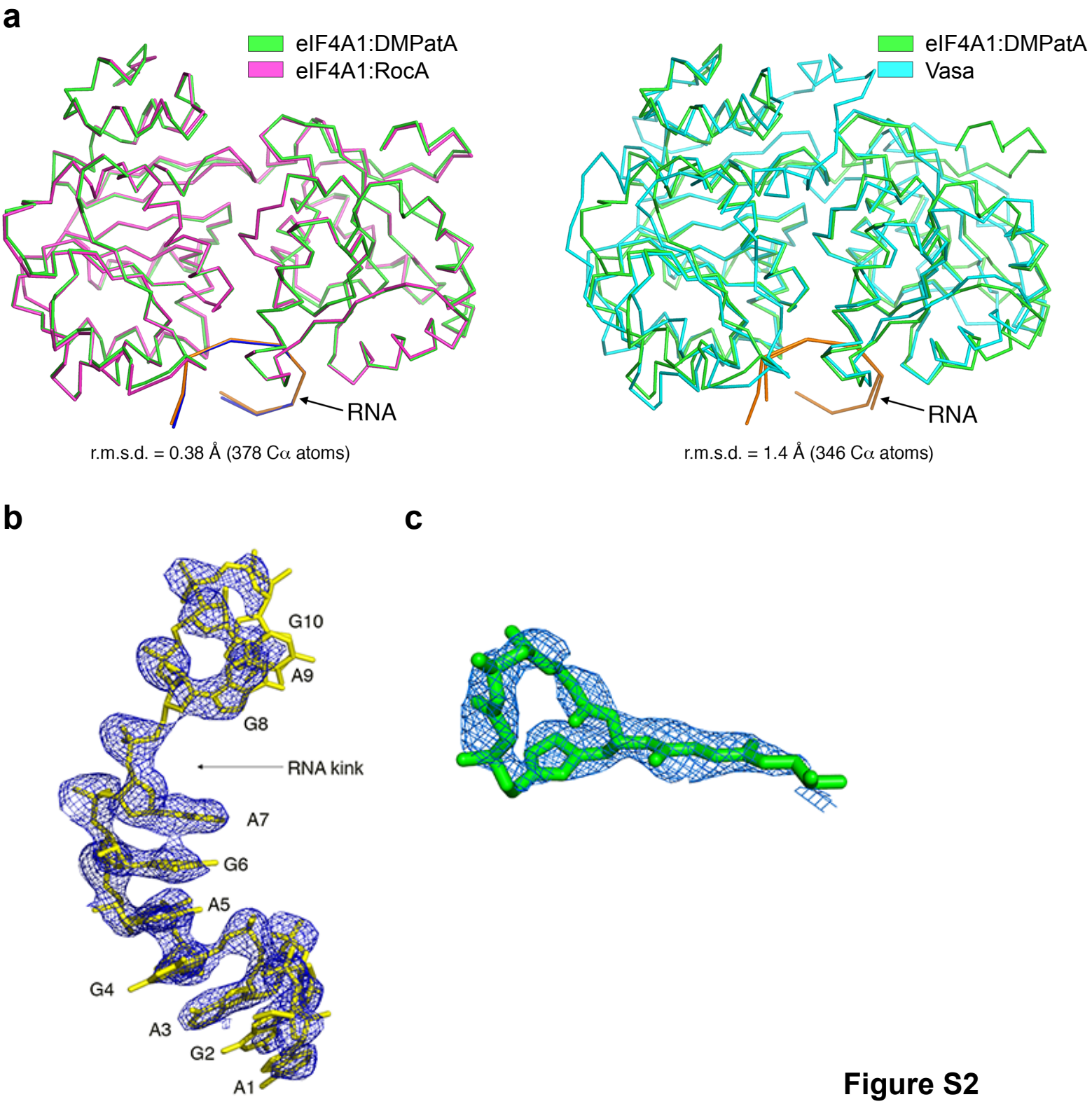
a
eIF4A1:DMPatA
eIF4A1:RocA
RNA
r.m.s.d. = 0.38 Å (378 Cα atoms)
eIF4A1:DMPatA
Vasa
RNA
r.m.s.d. = 1.4 Å (346 Cα atoms)
b
G10
A9
G8
RNA kink
A7
G6
A5
G4
A3
G2
A1
c

Figure S2

a

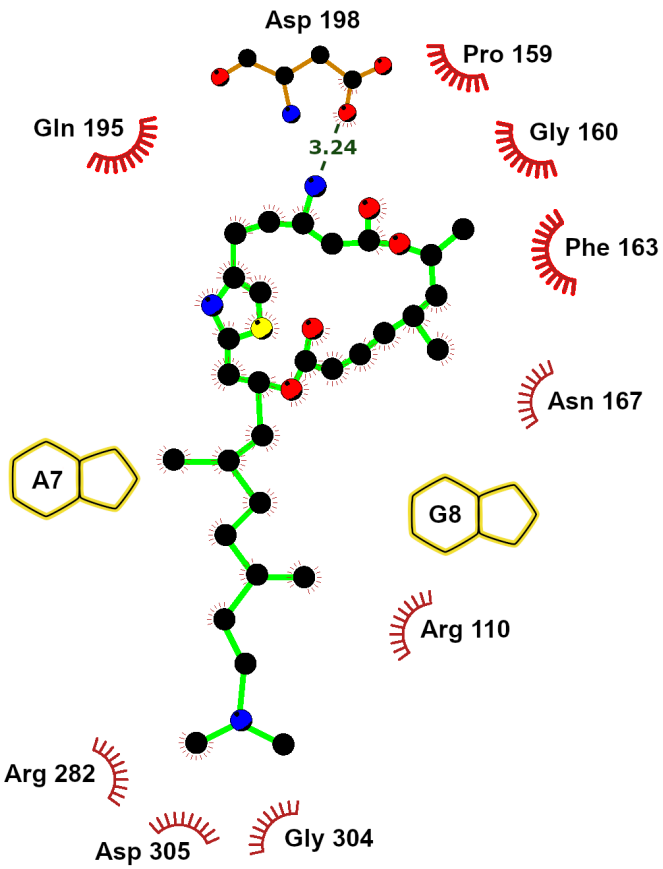

DMPatA

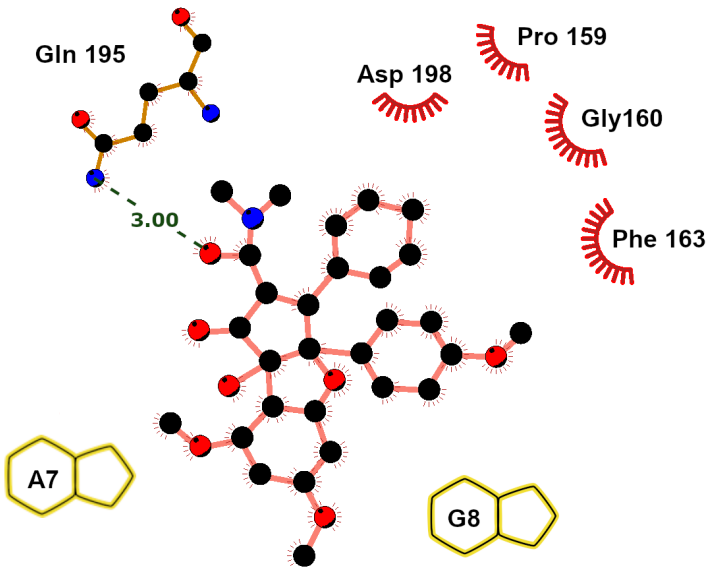

RocA

b

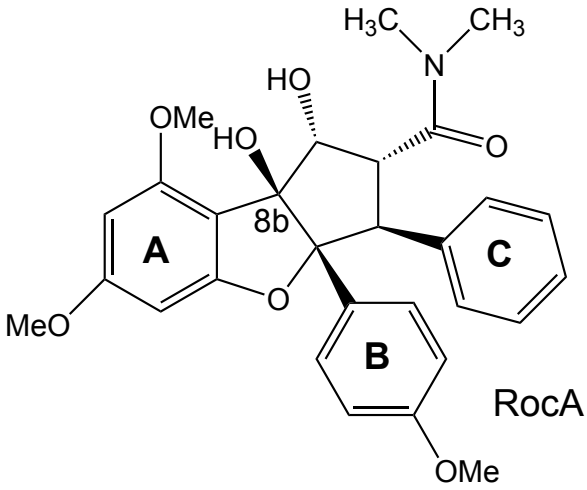

RocA

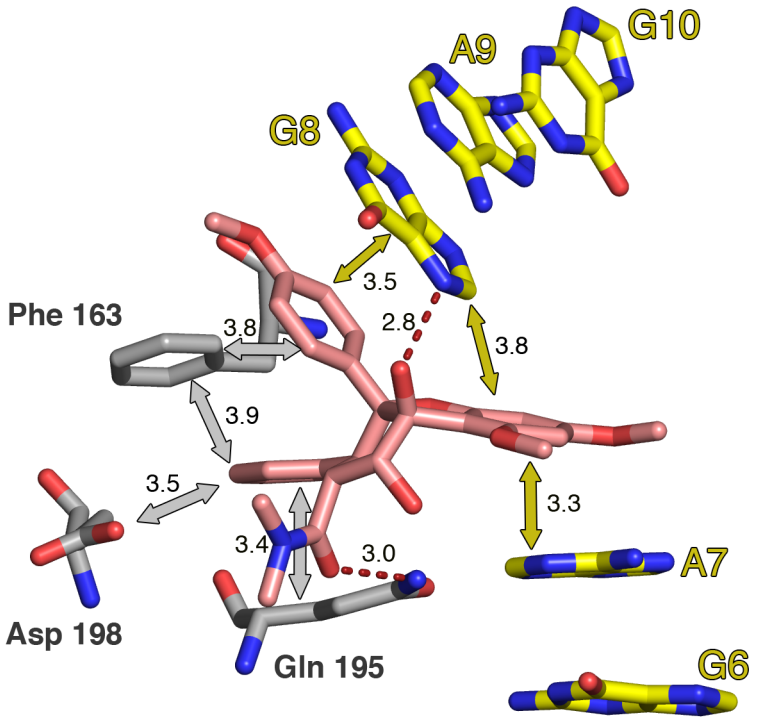

Figure S3

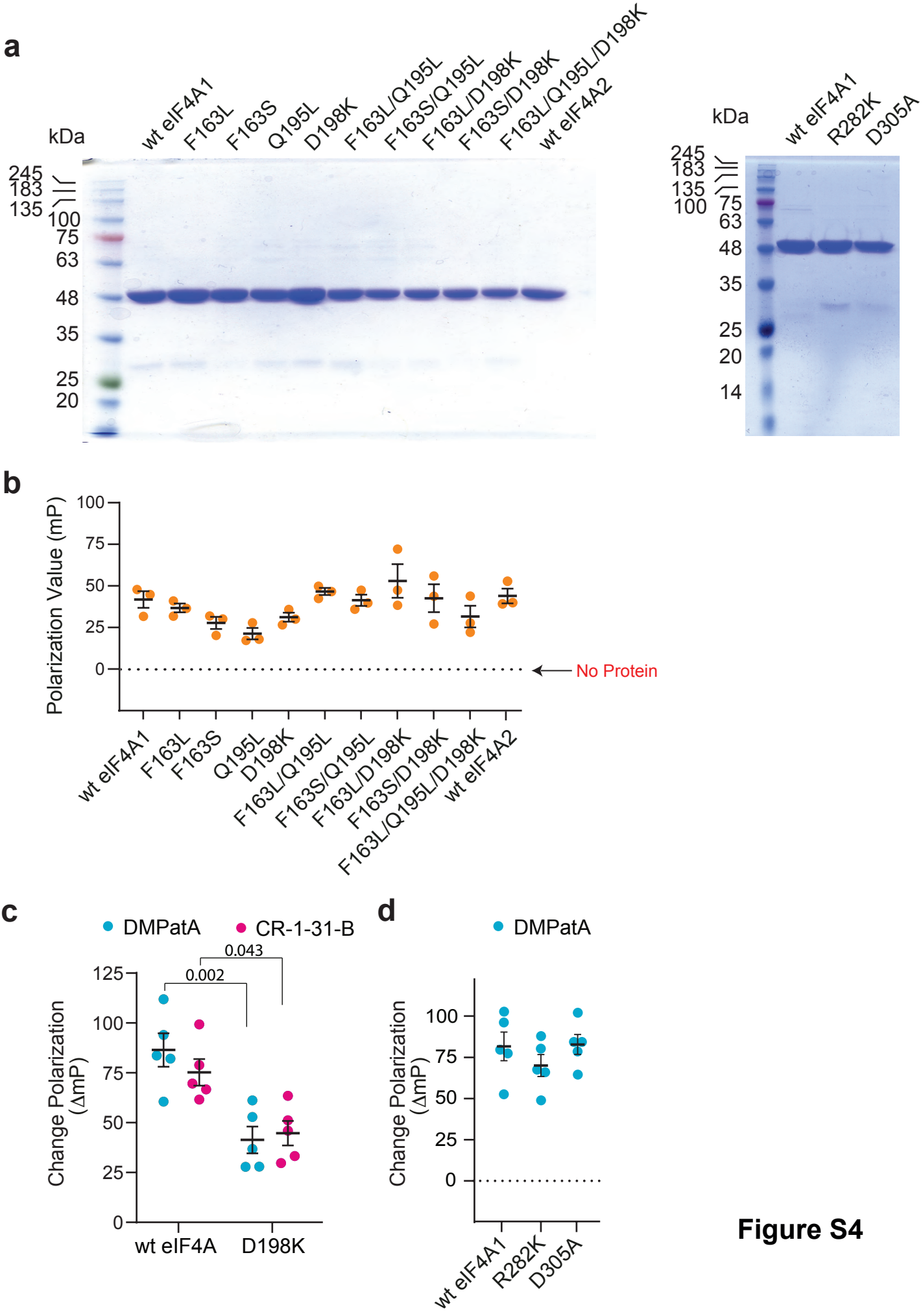
a
kDa
wt eIF4A1
F163L
F163S
Q195L
D198K
F163L/Q195L
F163S/Q195L
F163L/D198K
F163S/D198K
F163L/Q195L/D198K
wt eIF4A2
245
183
135
100
75
63
48
35
25
20
kDa
wt eIF4A1
R282K
D305A
245
183
135
100
75
63
48
35
25
20
14
b
Polarization Value (mP)
100
75
50
25
0
No Protein
wt eIF4A1
F163L
F163S
Q195L
D198K
F163L/Q195L
F163S/Q195L
F163L/D198K
F163S/D198K
F163L/Q195L/D198K
wt eIF4A2
c
DMPatA
CR-1-31-B
0.043
0.002
Change Polarization (ΔmP)
125
100
75
50
25
0
wt eIF4A
D198K
d
DMPatA
Change Polarization (ΔmP)
100
75
50
25
0
wt eIF4A1
R282K
D305A

Figure S4

a

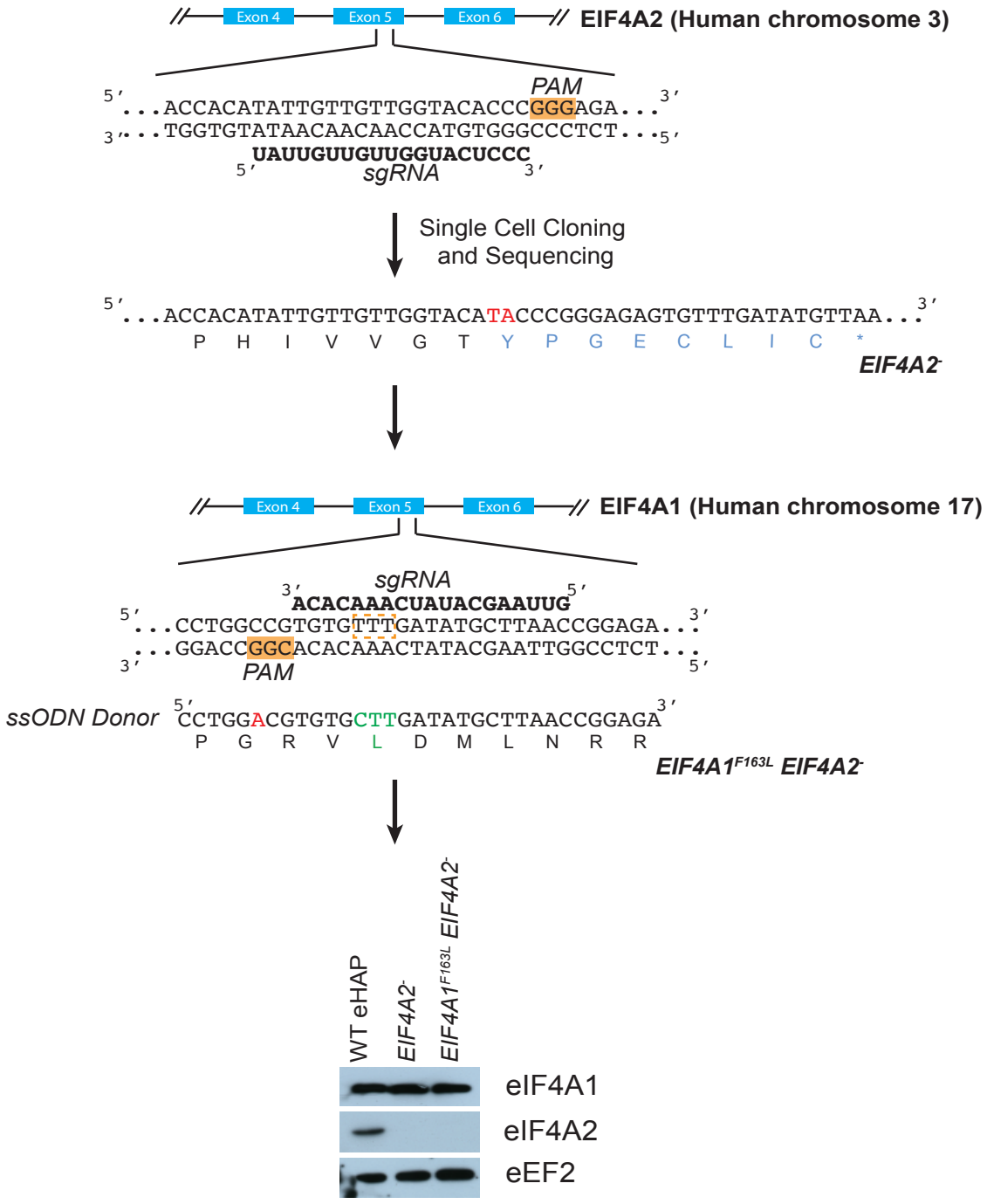
Exon 4
Exon 5
Exon 6
EIF4A2 (Human chromosome 3)
PAM
5′...ACCACATATTGTTGTTGGTACACCCGGGAGA...3′
3′...TGGTGTATAACAACAACCATGTGGGCCCTCT...5′
UAUUGUUGUUGGUACUCCC
5′ sgRNA 3′
Single Cell Cloning
and Sequencing
5′...ACCACATATTGTTGTTGGTACATACCCGGGAGAGTGTTTGATATGTTAA...3′
P H I V V G T Y P G E C L I C *
EIF4A2-
Exon 4
Exon 5
Exon 6
EIF4A1 (Human chromosome 17)
3′ sgRNA 5′
ACACAAACUAUACGAAUUG
5′...CCTGGCCGTGTGTTTGATATGCTTAACCGGAGA...3′
3′...GGACCGGCACACAAACTATACGAATTGGCCTCT...5′
PAM
ssODN Donor 5′ CCTGGACGTGTGCTTGATATGCTTAACCGGAGA 3′
P G R V L D M L N R R
EIF4A1F163L EIF4A2-
WT eHAP
EIF4A2-
EIF4A1F163L EIF4A2-
eIF4A1
eIF4A2
eEF2

b

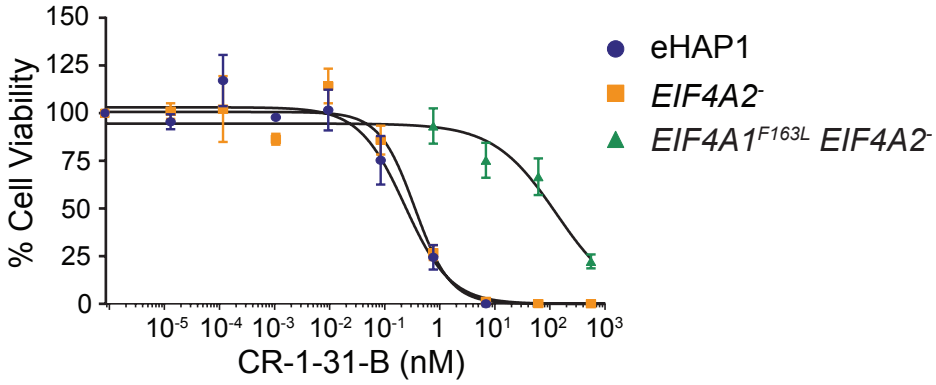
% Cell Viability
150
125
100
75
50
25
0
10-5 10-4 10-3 10-2 10-1 1 101 102 103
CR-1-31-B (nM)
eHAP1
EIF4A2-
EIF4A1F163L EIF4A2-

Figure S5